

Aurophilic Interactions in [L Au X]...[L' Au X] Dimers: Calibration by Experiment and Theory

Erik Andris,[†] Prokopis Andrikopoulos,[‡] Jiří Schulz,[†] Jan Turek,[§] Aleš Růžička,^{§,*} Jana Roithová,^{†,*} and Lubomír Rulíšek^{‡,*}

[†] Department of Organic Chemistry, Faculty of Science, Charles University, Hlavova 2030, 128 43 Prague 2, Czech Republic.

[‡] Institute of Organic Chemistry and Biochemistry, Czech Academy of Sciences, Flemingovo náměstí 2, 166 10 Prague 6, Czech Republic.

[§] Department of General and Inorganic Chemistry, Faculty of Chemical Technology, University of Pardubice, Studentská 573, CZ-532 10, Pardubice, Czech Republic

* Corresponding authors: rulisek@uochb.cas.cz; roithova@natur.cuni.cz; ales.ruzicka@upce.cz

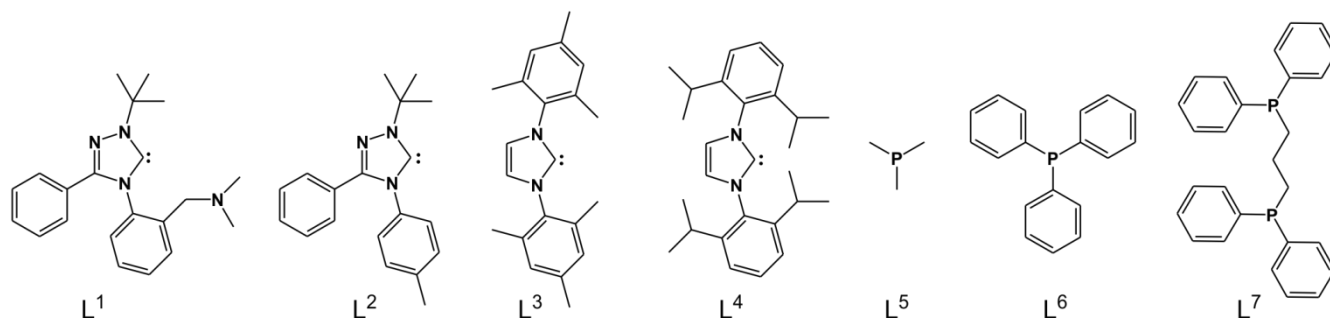
ABSTRACT: Attractive metallophilic (aurophilic, argentophilic, cuprophilic, ...) interactions play an important role in arrangement and stabilization of oligonuclear metal ion complexes. We report a combined experimental and theoretical assessment of aurophilic interactions in closed-shell gold(I) dimers. The experimental binding energies were obtained for charged [(LH)AuCl]⁺...[(L')AuCl] dimers (L is either a phosphine or a *N*-heterocyclic carbene ligand) in the gas phase. These energies served for benchmarking of correlated quantum chemical calculations (CCSD(T)-calibrated SCS-MP2/CBS method) that were then applied to neutral [(L)AuX]...[(L')AuX] dimers (X = Cl, Br, I). The overall attractive interactions between monomeric units are in the order of 100–165 kJ mol⁻¹ in the charged dimers and of 70–105 kJ mol⁻¹ in the corresponding neutral dimers. In the neutral dimers, pure aurophilic interactions account for 25–30 kJ mol⁻¹, the dipole-dipole interactions for 30–45 kJ mol⁻¹, and the L...L' “inter-ligand” dispersion interactions for 5–25 kJ.mol⁻¹. Energy of the aurophilic interactions is thus comparable or even larger than that of strong hydrogen bonds.

1. Introduction

Closed-shell metallophilic interactions are responsible for the formation of the metal-metal bound dimers or polynuclear metal clusters.^{1,2} Almost thirty years ago, Schmidbaur observed the first gold(I) complexes displaying short Au...Au distances in the solid state.³⁻⁵ His work paved the way for the ever-growing research on compounds exhibiting metallophilic interactions.⁶⁻⁹ For example, it was proposed that aurophilic interactions are important in materials science,¹⁰ medicinal chemistry,¹¹⁻¹⁴ and catalysis.¹⁵⁻²⁴ Pyykkö and coworkers pioneered theoretical investigation of aurophilic interactions.²⁵ They analyzed the role of intermolecular electrostatic, induction, and dispersion interactions in the overall attraction of closed-shell Au(I)...Au(I) dimers.²⁶ They also investigated the effect of a neutral ligand L in [(L)AuCl]₂.²⁶ Accurate treatment of the metallophilic interactions necessitated correlated *ab initio* methods, such as second order Møller-Plesset perturbation method (MP2) or coupled clusters method (CC).²⁵ Conversely, standard density functional theory (DFT) methods fail to provide satisfactory results. Andrejić and Mata used local correlation methods; local coupled clusters method LCCSD[T0] for small systems and local version of the spin-component scaling MP2 method (SCS-LMP2) for the rest.²⁷ These methods with appropriate localization schemes provided a decomposition of the interaction energies into spatial domains; e.g., separation of gold, chlorine and ligand interactions in the [(L)AuCl]₂ dimers. Moreover, the SCS-LMP2 interaction energies were almost quantitatively correct with respect to the benchmark LCCSD[T0] values. Andrejić and Mata further advocated in favor of the dispersion-corrected DFT methods in cases when *ab initio* correlated calculations cannot be afforded.²⁷ De Proft and co-workers investigated a large set of dimers formed from coinage metal complexes with an *N*-heterocyclic carbene ligand and a halogen counter ion.²⁸ All these studies led to the conclusion that the Au–Au binding energy is in the range of 20-65 kJ mol⁻¹. This energy range corresponds to weak forces and is comparable with that of hydrogen bonding.

The above studies represent the current state of the art in theoretical investigations of metallophilic interactions and set the guidelines for further computational studies. However, experimental benchmarks are missing. The ideal benchmarking experiment should provide the binding energy in an isolated [(L)AuX]₂ dimer in vacuum. This goal cannot be achieved with available experimental methods. However, it is possible to obtain bond dissociation energies in charged complexes.^{29,30} Herein, we studied [(L¹)AuCl] complex bearing *N*-heterocyclic carbene ligand L¹ (**Scheme 1**) with easily protonable tertiary amine group. We investigated a series of charged dimers [(L¹H)AuCl]⁺...[(L^{*n*})AuCl] (L^{*n*} = L¹ – L⁶, L⁷AuCl, see **Scheme 1**) and determined the experimental binding energies between the monomeric units. These energies were then compared with calibrated

high-level quantum chemical calculations (SCS-MP2 method benchmarked against CCSD(T) method). Finally, we separated the overall obtained interaction energies between the ion-neutral $[(L^1H)AuCl]^+ \dots [(L^n)AuCl]$ and neutral-neutral $[(L^1)AuCl] \dots [(L^n)AuCl]$ species into various contributions and were singled out “pure” aurophilic interactions from the dipole-dipole and ligand-ligand (through space) interactions.



Scheme 1. The ligands investigated in this study.

2. Experimental details

The $[(L^1)AuCl]$ and $[(L^2)AuCl]$ complexes were prepared according literature procedures.³¹ Complexes $[(L^n)AuCl]$ for $n = 3 - 6$ and ligand L^7 were obtained from commercial sources.

Mass spectrometry experiments were performed using quadrupole-octopole-quadrupole tandem mass spectrometer TSQ 7000 equipped with an electrospray ionization (ESI) source.^{32,33} The clusters were generated by electrospray ionization of 1 mM methanolic solutions of $[(L^n)AuCl]$ ($n = 2 - 7$, see Scheme 1) with three equivalents of $[(L^1)AuCl]$ and 10 equivalents of HCl (**Figure S3**). The ions of interest were mass-selected by the first quadrupole and collided in an octopole collision cell at variable collision energies with xenon at 40 °C and at typical pressures 0.2, 0.1, and 0.05 mTorr, measured with 120 AA Baratron (MKS instruments). The ionic products were mass-analyzed by the second quadrupole and detected using a Daly-type detector. The second quadrupole was kept at the offset corresponding to the sum of the first quadrupole and the octopole offsets. The nominally zero collision energy and the shape of the kinetic energy distribution were determined from the stopping potential analysis (**Figure S1**).³² The thermalization of the generated ions was tested by their collisional cooling in an additional collision cell placed to the region of a transfer quadrupole in the ESI source region. Because we did not detect any change in the evaluated data, we collected the data without this additional collisional thermalization.

The reaction cross-section for i -th dissociation channel σ_i was calculated as follows,

$$\sigma_i d \ell = -\ln(1 - \Sigma I_n / (\Sigma I_n + I_P)) I_i / \Sigma I_n \quad (1),$$

where d is the gas number density in the collision cell, $d = p/k_B T$ (T is the collision cell temperature (313.15 K), p is the collision gas pressure, and k_B is the Boltzmann constant), ℓ is the collision cell length (18.5 cm), ΣI_n is a sum of the intensities of all product ions, I_P is the intensity of parent ions and I_i is the intensity of ions belonging to the i -th channel. Each of the cross-section measurements was repeated at least three times on different days. The zero-pressure dissociation curve was extrapolated from the pressure dependence of normalized dissociation curves, (**Figure S2**) and fitted with a modified version of the L-CID program (**Figures S4–S10**).³⁰ The modifications of the fitting program account for the spontaneous decomposition of ions from the high-energy tail of their internal energy distribution. In addition, the ion kinetic energy broadening function was set to Lorentzian, which better describes the experimentally measured distribution (cf. **Figure S1**).³⁴ A full account of the changes to the L-CID program is described in the Supporting Information. We note that in the L-CID program, the nature of the transition structure assumed for a given dissociation channels has to be specified. It can be either loose (usually for neutral ligand elimination) or tight (dissociations proceeding via entropically constrained transition structures). The cluster cleavage described here as well as HCl elimination were modelled with the “loose” option, which provided results in good agreement with the observed branching ratios (i.e. the branching ratios can be rationalized based on the determined appearance energies for both channels). Additional support comes from the theoretical calculations that localized transition structures for HCl elimination with imaginary frequencies smaller than $i100 \text{ cm}^{-1}$. Furthermore, the L-CID requires specification of a number of free rotors in the molecule. This was assumed to be equal to the number of methyl groups in each complex (**Table S1**). We ran the L-CID simulation 16 times on each set of data (both dissociation channels were fitted simultaneously). The reported energies were calculated as an average of the energies obtained, when the genetic algorithm of the L-CID converged and the results fitted the experimental data. We tested the hypothesis that the two dissociation channels originate from different isomers of the parent ions and fitted them independently by L-CID. This fitting did not converge in most cases.

Infrared photodissociation spectra were acquired with the ISORI instrument, equipped with an ESI ion source from the TSQ 7000,³⁵ and Nd:YAG-pumped IR optical parametric oscillator/amplifier system from LaserVision calibrated by WS-600 wavelength meter from HighFinesse GmbH as the IR light source. The generated ions were mass-selected by first quadrupole and captured by a helium pulse

in a cryogenic (3 K) linear quadrupole ion trap. At these conditions, the ions form weakly bound $[\text{M.He}]^+$ complexes. The absorption of the IR light by the complexes was monitored by comparing two filling cycles. To obtain the base count N_{i0} , the ions were stored for a specified amount of time, ejected from the trap, mass-selected for the $[\text{M.He}]^+$ by second quadrupole and counted. To obtain the wavelength-dependent ion count N_i , the above sequence was repeated, but this time, the contents of the trap were irradiated by IR light, which caused, upon absorption, depletion of the $[\text{M.He}]^+$ complexes. The IR spectra were then plotted as $1 - N_i / N_{i0}$.³⁶

3. Computational details

We performed the calculations using the Turbomole 7.1 program.³⁷ Geometry optimizations were carried out at the DFT level, employing the Perdew-Burke-Ernzerhof (PBE) functional,³⁸ which included Grimme's dispersion correction³⁹ in its version 3 (PBE-D3) and the def2-SVP basis set on all of the atoms.^{40,41} Along with the PBE-D3 geometry optimization, we have also carried out optimization at the TPSS⁴²-D3/def2-SVP level and for one model system also at the B3LYP⁴³-D3/def2-SVP level. The resulting equilibrium geometries differed only marginally which is further indication of the robustness of the adopted protocol and of the reliability of the results obtained. Moreover, the obtained SCS-MP2/CBS interaction energies (*vide infra*) for separation of the dimer into the monomers computed for the $[(\text{L}^1\text{H})\text{AuCl}]^+ \dots [(\text{L}^5)\text{AuCl}]$ system at PBE versus B3LYP equilibrium geometries only differed by less than 1 kJ.mol⁻¹. Most of the reported interaction energies were obtained as single-point energies using the spin-component scaling second order Moller-Plesset perturbation method (SCS-MP2) with the recommended $\text{cos} = 6/5$ and $\text{css} = 1/3$ parameters⁴⁴ and extrapolated to the complete basis set limit (CBS) using the aug-cc-pVDZ and aug-cc-pVTZ basis sets,⁴⁵ and the Helgaker's formula⁴⁶:

$$E^{\text{MP2/CBS}[D:T]} = E^{\text{HF}/\text{aug-cc-pVTZ}} + \frac{3^3 E^{\text{MP2}_{\text{corr}}/\text{aug-cc-pVTZ}} - 2^3 E^{\text{MP2}_{\text{corr}}/\text{aug-cc-pVDZ}}}{3^3 - 2^3} \quad (2a);$$

$$E^{\text{MP2/CBS}[T:Q]} = E^{\text{HF}/\text{aug-cc-pVQZ}} + \frac{4^3 E^{\text{MP2}_{\text{corr}}/\text{aug-cc-pVQZ}} - 3^3 E^{\text{MP2}_{\text{corr}}/\text{aug-cc-pVTZ}}}{4^3 - 3^3} \quad (2b).$$

The Hartree-Fock energy is not extrapolated but taken from the calculation in the larger basis set used for the extrapolation, whereas the $E^{\text{MP2}_{\text{corr}}}$ denotes the MP2 correlation energy, i.e. $(E^{\text{MP2}_{\text{tot}}/\text{BS}} - E^{\text{HF}/\text{BS}})$ in the given basis set (BS).

The accuracy of SCS-MP2 energies was validated by its benchmarking against the reference CCSD(T) method on a set of smaller model complexes. At the same time, the performance of several popular DFT functionals - B3LYP,⁴³ TPSS,⁴² and PBE³⁸ - was investigated as well (both with and without the D3 dispersion correction). In these benchmark calculations, the def2-TZVP⁴¹ and aug-cc-pVTZ⁴⁷ basis sets were employed. All calculations (both DFT and wave function) were expedited by expanding the Coulomb integrals in an auxiliary basis set, the resolution-of-identity, RI-J (or density-fitting, DF) approximation,^{48,49} or RI-JK in case of Hartree-Fock method, wherever possible. It was carefully checked that the two adopted RI approximations have only marginal effect on the final interaction energies, ~ 0.2 kJ.mol⁻¹. The standard Boys-Bernardi counterpoise correction method was used to estimate the basis set superposition error (BSSE) and the interaction energies also account for the relaxation of the monomers. The BSSE accounts for $\sim 35\%$ of the overall interaction energies of the investigated complexes at the SCS-MP2/aug-cc-pVTZ level of calculation. Therefore, the BSSE-uncorrected values are quite meaningless and far from the experimental values.

The zero-point vibrational energy (ΔE_{ZPVE}), thermal contributions to enthalpy and entropic contributions at 298 K and 1 bar (10⁵ Pa) were calculated using the analytical harmonic vibrational frequencies calculated at the RI-PBE-D3/def2-SVP level.⁵⁰ Infrared spectra predictions were performed at B3LYP-D3/def2-SVP level of theory.

4. Results

4.1. Mass spectrometry experiments. Electrospray ionization of a solution of gold(I) complexes with ligand L¹ and one of the ligands L¹–L⁷ generated the desired [(L¹H)(Lⁿ)Au₂Cl₂]⁺ complexes with protonated L¹. The complex structures most likely correspond to the [(L¹H)AuCl]⁺...[(Lⁿ)AuCl] dimers (note that L⁷ is a bisphosphine ligand and thus coordinates two AuCl units - therefore $n = 7$ in a listing refers to the cluster [(L¹H)AuCl]⁺...[(L⁷)Au₂Cl₂]⁺). This assumption was verified for the [(L¹H)AuCl]⁺...[(L¹)AuCl] complex by measuring its infrared photodissociation (IRPD) spectrum (Figure 1a). IR spectra of possible isomers of [(L¹H)AuCl]⁺...[(L¹)AuCl] differ mainly in positions of the bands associated with the proton (*cf.* Figure 1b and Figure S13). Hence, we measured IRPD spectra of protonated as well as deuterated dimer (blank and blue spectra in Figure 1a). The bands associated with protonation can be visualized as the difference spectrum (Figure 1a, pink trace). The difference spectrum shows a broad band at 2680 cm⁻¹, followed by a band at 2760 cm⁻¹ and a continuum, featuring another maximum at 2930 cm⁻¹ ending below 3000 cm⁻¹.

Protonation site and binding between the monomeric units can be deduced by comparing the experimental bands associated with the protonation and the theoretical IR spectra. We can exclude the proton binding to chlorine or gold atoms, because stretching vibrations of such bonds would be located at lower wavenumbers than experimentally observed. The alternative protonation at the nitrogen atom has to be associated with further hydrogen bonding, because the free N-H stretch would be located around 3400 cm^{-1} (**Figure S13c,f**). The only possibility is thus protonation at the amino group that is surrounded by possible hydrogen-bond acceptors. Further, we exclude interaction of the protonated amino group with the chlorine anion directly, because such interaction would redshift the N-H bond well below 2600 cm^{-1} (**Figure S13b,d**). The only structures consistent with the observed spectra are thus the expected dimeric clusters $[(L^1H)AuCl]^+ \dots [(L^1)AuCl]$ (**Figure 1b-d**), in which the N-H unit is either bound to the chlorine atom in the Au-Cl unit of the other subunit (**Figure 1b,c**), or to the Au atom of the same subunit (**Figure 1d**). Also, theory predicts these structures as the lowest-energy isomers (**Figure S13**). We will not further attempt to assign the experimental spectrum to one, two, or all of these three isomers, because the main goal of this work is calibration of energetics and it is almost the same for all of them. The assignment would be complicated due to the diffuse character of the N-H band (**Figure 1a**, pink trace) which is typical for stretches involving hydrogen bonds. Moreover, we probably observe a whole progression of these vibrational bands.

The lower frequency range is dominated by ligand vibrations. The ligand vibrations are very little affected by the interaction between the monomeric units. Therefore, the lower frequency range offers little or no information on how the units in the dimeric cluster interact.

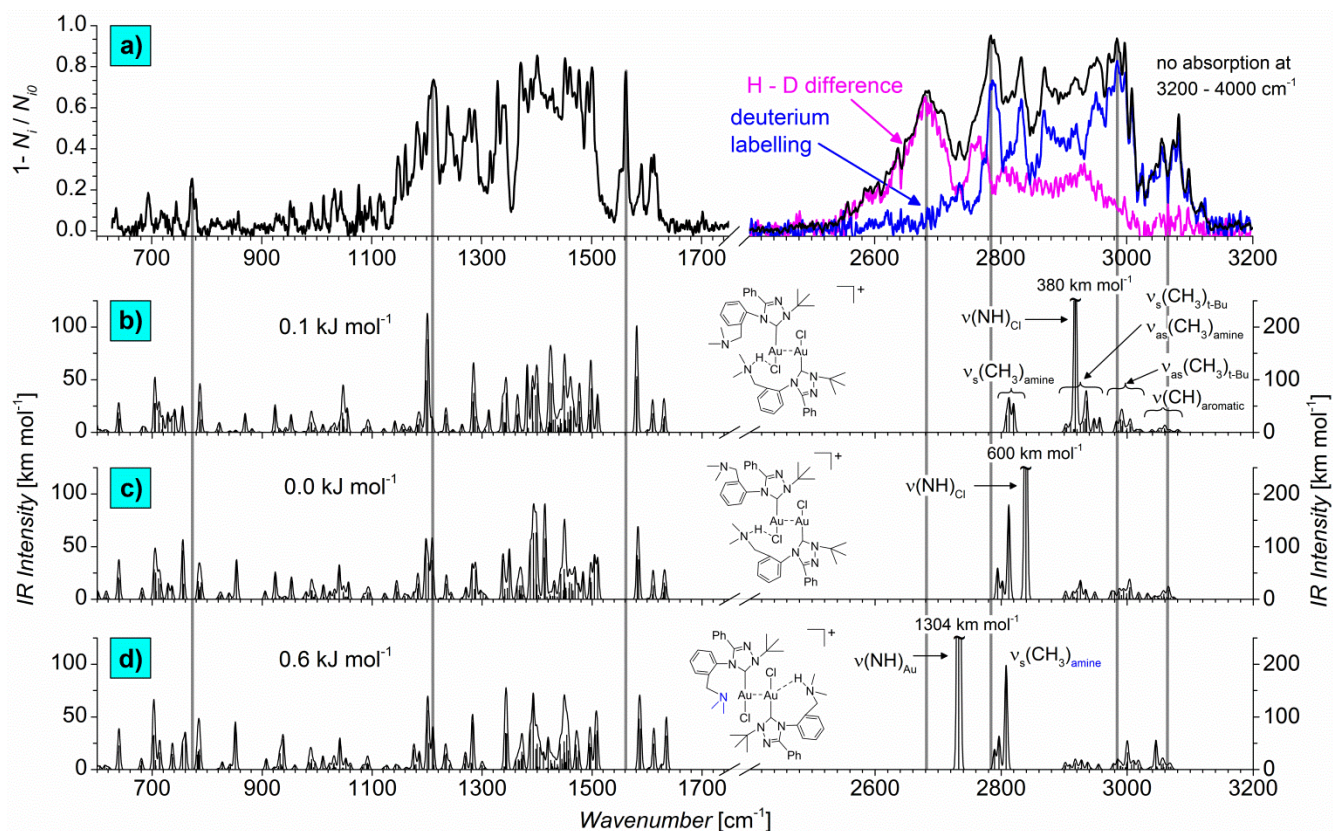
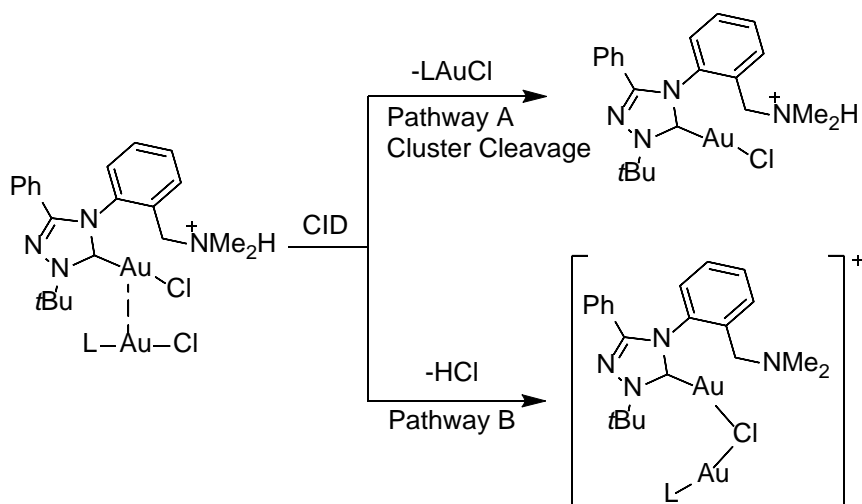


Figure 1. a) Helium tagging infrared photodissociation spectra of the $[(L^H)AuCl]^+ \dots [(L^1)AuCl]$ (black trace) and $[(L^D)AuCl]^+ \dots [(L^1)AuCl]$ (blue trace) complexes. The pink trace shows the difference spectrum (pink trace). b-d) Theoretical IR spectra and relative energies (at 0 K) of different dimeric clusters calculated with B3LYP-D3/def2-SVP. Additional isomers are shown in [Figure S13](#). The frequency scaling factors of 0.98 and 0.955 were used in the lower and upper frequency range and were chosen to fit the NHC ligand bands.⁵¹

Collision induced dissociation (CID) of the $[(L^H)AuCl]^+ \dots [(L^n)AuCl]$ clusters led to the cluster cleavage, forming the mononuclear complexes $[(L^H)AuCl]^+$ and $[(L^n)AuCl]$ ([Scheme 2](#), Pathway A). We observed this fragmentation pathway in competition with HCl elimination ([Scheme 2](#), Pathway B). The branching ratios between the cluster cleavage and the HCl elimination were drastically dependent on the collision energy ([Figure 2](#)). For most complexes, the HCl elimination was the dominant fragmentation process at small collision energies (e.g. in [Figure 2](#)). At large collision energies, cluster cleavage plays a much more important role ([Figures S4–S10](#)). This suggests that HCl eliminates via a transition structure lying slightly below the energy required for the cluster cleavage. Hence, HCl elimination prevails at low collision energies, and becomes disfavored at high collision energies due to entropic reasons.



Scheme 2. Observed fragmentation pathways of the $[(L^1H)AuCl]^+ \dots [(L^n)AuCl]$ clusters ($n = 1 - 7$).

Next, we extracted the dissociation energies of the cluster cleavage as well as of the loss of HCl from the energy-dependent fragmentation curves of the $[(L^1H)AuCl]^+ \dots [(L^n)AuCl]$ clusters (**Table 1** and **Figure 2**, for details see the Supporting Information). We have used the L-CID program of Chen and co-workers to evaluate the curves.³⁰ This approach proved suitable for evaluating dissociation energies in metal-metal bound complexes.⁵² Chen also demonstrated that this method can address complexes bound by weak interactions.⁵³

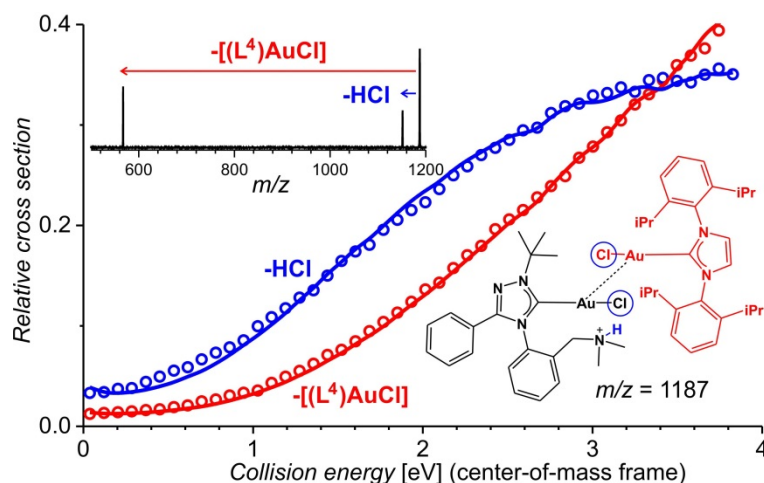
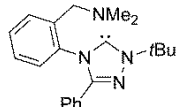
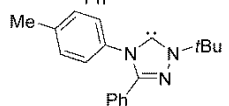


Figure 2. The energy dependence of the fragmentation yields in dissociation of the $[(L^1H)AuCl]^+ \dots [(L^4)AuCl]$ cluster (m/z 1187) to $[(L^1H)AuCl]^+$ (m/z 567) + $[(L^4)AuCl]$ and to $[(L^1)(L^4)Au_2Cl]^+$ (m/z 1151) + HCl. The experimental data (points) were fitted with the L-CID program (lines). The inset shows the CID spectrum at $P(Xe) = 0.04$ mTorr and $E_{coll} = 4$ eV.

Table 1. Experimental appearance energies^a (*AE*) of the fragmentation channels for the [(L¹H)AuCl]⁺...[(L^{*n*})AuCl] (*n* = 1 – 7) complexes studied.

Complex	L ^{<i>n</i>}	<i>AE</i> ([(L ¹ H)AuCl] ⁺) [kJ mol ⁻¹]	<i>AE</i> (HCl) [kJ mol ⁻¹]
[(L ¹ H)AuCl] ⁺ ...[(L ¹)AuCl]		134 ± 5	121 ± 6
[(L ¹ H)AuCl] ⁺ ...[(L ²)AuCl]		132 ± 5	121 ± 4
[(L ¹ H)AuCl] ⁺ ...[(L ³)AuCl]	IMes	147 ± 7	130 ± 6
[(L ¹ H)AuCl] ⁺ ...[(L ⁴)AuCl]	IPr	144 ± 7	128 ± 7
[(L ¹ H)AuCl] ⁺ ...[(L ⁵)AuCl]	Me ₃ P	102 ± 11	100 ± 12
[(L ¹ H)AuCl] ⁺ ...[(L ⁶)AuCl]	PPh ₃	123 ± 7	115 ± 8
[(L ¹ H)AuCl] ⁺ ...[(L ⁷)AuCl]AuCl]	Ph ₂ P(CH ₂) ₃ PPh ₂	154 ± 6 ^b	128 ± 5

^a The values were obtained by fitting the experimental CID curves using the L-CID program (see the SI for details). They are given in the center of mass reference frame. The uncertainties are the standard deviations of the mean of fits of the experimental data (always three independent experimental curves were analyzed).

^b The *AE* energy was associated with elimination of [(L⁷)Au₂Cl₂].

The L-CID simulation of all data provided smaller appearance energies (*AE*) for the HCl elimination than for the cluster cleavage. Further, both appearance energies grow with the size of the ligand L^{*n*} in [(L¹H)AuCl]⁺...[(L^{*n*})AuCl] (**Table 1, Figure 3a,b**). The largest energies are required for fragmentating clusters bearing *N*-heterocyclic carbene ligands IMes (L³) and IPr (L⁴), and the bisphosphine ligand (L⁷AuCl). The smallest *AE*s were observed for fragmentating [(L¹H)AuCl]⁺...[(L^{*n*})AuCl] with L^{*n*} being trimethylphosphine. Hence, the binding energies correlate with the size (mass) of the ligand L^{*n*} in [(L¹H)AuCl]⁺...[(L^{*n*})AuCl] (**Figure 3b**) which might be due to dispersion interactions.

The difference between the HCl elimination and cluster cleavage appearance energies correlates well with the relative abundance of the HCl elimination. Hence, the small *AE*s difference found for [(L¹H)AuCl]⁺...[(L⁵)AuCl] implicates almost complete kinetic suppression of HCl elimination. Conversely, for other clusters, HCl elimination demands approximately 10-20 kJ mol⁻¹ less energy than cluster cleavage and, therefore, HCl elimination prevails at lower collision energies (e.g. Figure 2).

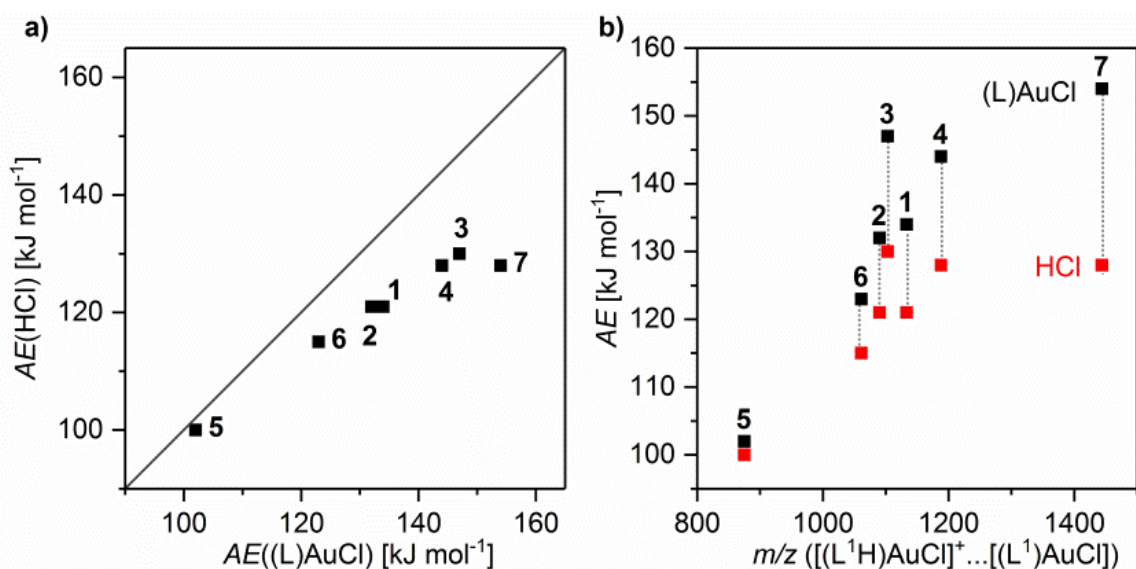


Figure 3. a) Correlation between the appearance energies for the HCl elimination and the appearance energies determined for the cluster cleavage of the $[(\text{L}^1\text{H})\text{AuCl}]^+ \dots [(\text{L}^n)\text{AuCl}]$ complexes ($n = 1 - 7$, n is denoted at each point in the graph). b) Dependence of the appearance energies of the HCl elimination (red points) and the cluster cleavage (black points) on the m/z ratio of parent complexes $[(\text{L}^1\text{H})\text{AuCl}]^+ \dots [(\text{L}^n)\text{AuCl}]$ ($n = 1 - 7$, n is denoted at each point in the graph). Note that $n = 7$ refers to $[(\text{L}^1\text{H})\text{AuCl}]^+ \dots [(\text{L}^7)\text{AuCl}]\text{AuCl}$ cluster.

4.2. Theoretical Calculations: calibration of the quantum chemical methods on the model

$[(\text{L})\text{AuCl}] \dots [(\text{L}')\text{AuCl}]$ dimers. Firstly, we have benchmarked various computational methods (both *ab-initio* and DFT methods) by calculation of the interaction energies in smaller model systems, some of them previously studied by other authors.²⁶⁻²⁸ The models include $[(\text{N}_2\text{C})\text{AuCl}]_2$, $[(\text{N}_2\text{C})\text{AuCl}] \dots [(\text{H}_3\text{P})\text{AuCl}]$, $[(\text{NHC})\text{AuCl}] \dots [(\text{N}_2\text{C})\text{AuCl}]$, $[(\text{NHC})\text{AuCl}] \dots [(\text{H}_3\text{P})\text{AuCl}]$, $[(\text{NHC}^{\text{CT}})\text{AuCl}]^+ \dots [(\text{N}_2\text{C})\text{AuCl}]$, $[(\text{NHC}^{\text{CT}})\text{AuCl}]^+ \dots [(\text{H}_3\text{P})\text{AuCl}]$, and $[(\text{H}_3\text{P})\text{AuCl}]_2$ homo- or heterodimers, where N_2C stands for 3*H*-diazirine-ylidene, NHC stands for 1,4-dihydro-5 λ^2 -1,2,4-triazole (the core 1,2,4-triazole ring present in ligands **1** and **2**; the aryl/alkyl substituents are replaced by hydrogen atoms). The charge-tagged NHC ligand (NHC^{CT}) bears the protonated $\text{NH}_3^+\text{CH}_2^-$ group at position 4. We optimized the geometries at the PBE-D3/def2-SVP level (Figure S12). Our key aim is the direct comparison between theoretical and experimental data, therefore we assessed the performance of the quantum chemical methods mostly for experimentally relevant structures corresponding to the global minima on the respective potential energy surfaces.

One important aspect concerning the aurophilic interactions, thoroughly discussed in the previous studies^{26,28} is the orientation of the monomers in the $[(\text{L})\text{AuCl}]_2$ dimers. In order to suppress

the leading dipole-dipole interaction term and single out the “pure” gold(I)-gold(I) interactions, the dimers are often considered in a constrained perpendicular orientation of the linear L-Au-Cl monomeric units.²⁶ However, the global minima on the potential energy surface are almost always characterized by an antiparallel orientation of the monomeric units, evidenced also by the existing crystal structures (for example in References 54, 55) and as found for our clusters as well (**Figure S12**). We have constrained the perpendicular orientation of the monomers only for a few model dimers in order to estimate “pure” aurophilic interactions (**Table 2**, bottom). The reader interested in a detailed computational investigation of the orientational dependence of the interacting closed-shell metal dimers is referred to the work of Straka and Pyykkö.⁵⁶

Table 2. The calculated BSSE-corrected interaction energies (ΔE_{int}) for the model [(L)AuCl]...[(L')AuCl] dimers.^a

L ...L'	CCSD(T) (aDZ) ^b	SCS-MP2 (aDZ)	ΔCC_{aDZ}^c	CCSD(T) (aTZ) ^b	SCS-MP2 (aTZ)	ΔCC_{aTZ}	SCS-MP2 CBS[D:T]	SCS-MP2 CBS[T:Q]
N ₂ C...N ₂ C	-39.2	-39.7	-0.5	-49.3	-48.3	1.0	-52.4	-55.9
N ₂ C...H ₃ P	-52.6	-53.2	-0.6	-61.2	-60.2	1.0	-63.8	-66.8
N ₂ C...NHC	-81.6	-80.2	1.4				-94.7	-98.0
NHC...H ₃ P	-88.6	-87.5	1.1				-99.0	-101.1
NHC ^{CT} ...N ₂ C ^d	-85.3	-85.6	-0.3				-96.4	-99.2
NHC ^{CT} ...H ₃ P	-105.4	-105.0	0.4				-115.5	-118.1
NHC ^{CT} ...N ₂ C (HCl _{association}) ^e	-26.4	-26.5	-0.1		-20.0		-21.7	-15.5
NHC ^{CT} ...H ₃ P (HCl _{association})	-20.9	-20.5	0.4		-15.5		-17.1	-9.9
H ₃ P...H ₃ P	-64.4	-65.4	-1.0	-71.8	-71.2	0.6	-74.4	-77.0
N ₂ C...N ₂ C ^{90°f}							-22.1	-23.1
N ₂ C...H ₃ P ^{90°}							-28.0	-29.3
H ₃ P...H ₃ P ^{90°}							-29.3	-30.6

^a All values are in kJ mol⁻¹

^b aDZ/aTZ stands for the aug-cc-pVDZ/aug-cc-pVTZ basis sets, respectively.

^c difference from the CCSD(T) level.

^d NHC^{CT} = charge-tagged ligand (4-NH₃⁺CH₂)NHC

^e BSSE uncorrected interaction energy for the [(NHC^{CT})Au₂Cl]⁺ + HCl → [(NHC^{CT})AuCl]⁺...[(L')AuCl] dissociation channel (the sign of ΔE_{int} corresponds to an association as exemplified by the above equation)

^f The interaction energy for the perpendicular orientation of the L-Au-Cl...L'-Au-Cl units

The calculated interaction energies (**Table 2**) show that in all cases the SCS-MP2 values quantitatively agree with the reference CCSD(T) values (the mean absolute deviation is 0.6 kJ mol⁻¹, whereas maximum absolute deviation is 1.4 kJ mol⁻¹), both in the aug-cc-pVDZ (all model systems) and in the aug-cc-pVTZ (for X/Y = PH₃, :CN₂) basis sets. This allowed us to conveniently investigate the convergence with respect to the basis set employing much cheaper SCS-MP2 method and aug-cc-pVXZ basis sets (X = D, T, Q; c.f. Equations 2a,b). It can be seen that the SCS-MP2/CBS[T:Q] values are 2-3 kJ mol⁻¹ more negative than SCS-MP2/CBS[D:T] values (that are affordable for the target systems) and thus we may conclude that the latter values used throughout this work will very slightly underestimate the interaction between [(L)AuCl] and [(L')AuCl] monomers. Surprisingly, the opposite is true for the HCl dissociation channel (these are BSSE uncorrected values for the two model systems and expectedly, the convergence with the basis set might be slower). Finally, the SCS-MP2/CBS[T:Q] and SCS-MP2/CBS[D:T] values for the interaction energies of the [(L)AuCl] and [(L')AuCl] monomers in the perpendicular orientation of the L-Au-Cl and L'-Au-Cl bonds differ by only 1 kJ mol⁻¹ (last three rows in **Table 2**). The perpendicular orientation of the units decreases the interaction energy in the dimer (23-30 kJ mol⁻¹ vs. 56-118 kJ mol⁻¹) and therefore also these deviations are smaller than for the fully optimized structures.

On the contrary, all tested DFT(-D3) and MP2 (including SOS-MP2) methods failed to agree with the benchmark CCSD(T) calculations. They tended to overestimate the aurophilic interactions by 15-45%. It can thus be concluded that from all the studied methods, SCS-MP2 is apparently the only method that may be capable of providing quantitatively accurate results for the target systems which are way beyond the computational feasibility of the CCSD(T) method and likely also beyond its DLPNO(TightPNO) variant⁵⁷, if we consider the CCSD(T) values as solid reference values.

Hence, we employed SCS-MP2/aug-cc-pVDZ and SCS-MP2/aug-cc-pVTZ levels and the extrapolation to the CBS for the calculations of the interaction and association (dissociation) energies of the target systems. Because of the size of the systems, we had to use the RI-JK/HF approximation to obtain the reference Hartree-Fock wave functions. We verified this approach on the smallest target systems - [(L¹H)AuCl]⁺...[(L⁵)AuCl] and [(L¹)AuCl]...[(L⁵)AuCl]. The errors introduced by the RI-JK/HF approximation on the final SCS-MP2 dissociation energies are negligible (0.1-0.2 kJ.mol⁻¹).

4.3. Interaction energies and enthalpies of the [(L¹H)AuCl]⁺...[(Lⁿ)AuCl] and [(L¹)AuCl]...[(Lⁿ)AuCl] dimers. Neutral dimers [(L¹)AuCl]⁺...[(Lⁿ)AuCl] almost exclusively adopt the expected antiparallel orientation of the linear L-Au-Cl units (**Figures 3 and S12**). On the contrary, protonated dimers [(L¹H)AuCl]⁺...[(Lⁿ)AuCl] and the products of the HCl elimination exist in a

multitude of conformations. Therefore, we started with several (5-15) conformations and geometrical arrangements for each of the protonated dimeric structures. Moreover, we ran 500 ps molecular dynamics trajectories at 500 K (employing the CUBY program and PM6-D3H4 semiempirical potential) for each dimer and submitted 50 snapshots from each trajectory to the quantum chemical calculations.⁵⁸ All the equilibrium geometries are deposited in Supporting Information and only several representative systems are depicted in **Figure 3**. These structural motifs are consistent with the experimental IR spectra of [(L¹H)AuCl]⁺...[(L¹)AuCl] dimer (**Figure 1**) and most of them are verified *a posteriori* by comparison of the computed interaction energies with the experimental data.

Table 3. The calculated SCS-MP2/CBS interaction (association) energies (ΔE_{int} , D_e) and enthalpies (ΔH_0) for the [(L¹H)AuCl]⁺...[(Lⁿ)AuCl] and [(L¹)AuCl]...[(Lⁿ)AuCl] dimers.^a

L'	[(L ¹)AuCl]...[(L ⁿ)AuCl]		[(L ¹ H)AuCl] ⁺ ...[(L ⁿ)AuCl]		[(L ¹ H)AuCl] ⁺ ...[(L ⁿ)AuCl]; HCl assoc	
	D_e	ΔH_0	D_e	ΔH_0 (AE_{exp}) ^b	D_e	ΔH_0
L ¹	-104.8	-102.3	-123.5	-117.4 (134 ± 5)	-83.8	-67.7
L ²	-109.3	-107.3	-131.0	-126.5 (132 ± 5)	-78.6	-62.8
L ³	-85.5	-84.0	-140.7	-134.1 (147 ± 7)	-107.6	-90.5
L ⁴	-91.7	-87.5	-138.5	-133.1 (144 ± 7)	-107.6	-94.3
L ⁵	-86.7	-84.6	-106.2	-102.3 (102 ± 11)	-113.2	-95.9
L ⁶	-90.5	-88.9	-112.4	-108.1 (123 ± 7)	-104.5	-88.6
L ⁷ ·AuCl ^c	-76.8	-74.4	-154.5	-149.2 (154 ± 6)	-110.3	-93.0

^a All values are in kJ mol⁻¹

^b $AE_{\text{exp}} \approx -\Delta H_0$

^c Note that L⁷ forms a complex with two gold atoms (see above); i.e. we always investigate the cluster [(L¹H)AuCl]⁺...[(L⁷AuCl)AuCl]

The calculated interaction energies/enthalpies are systematically larger for the protonated dimers [(L¹H)AuX]⁺...[(Lⁿ)AuX] than for their neutral counterparts (D_e and $\Delta H_{0\text{K}}$ in **Table 3**; $\Delta H_{298\text{K}}$ and $\Delta G_{298\text{K}}$ are in **Table S3**). Somewhat surprisingly we did not observe a strong correlation between the corresponding interaction energies obtained for the neutral and the protonated clusters. We attribute this to the difference in structural arrangements between the neutral and protonated dimers. In accordance with the experimental data, the calculations clearly show that the HCl dissociation channel (forming HCl and [(L¹)(Lⁿ)Au₂Cl]⁺) was thermodynamically preferred in all cases by 6-64 kJ mol⁻¹ to the cluster cleavage. We attempted to localize the corresponding transition structures for the

elimination of the HCl and calculated activation enthalpies - ΔH^\ddagger_0 , but the obtained values ([Table S3](#)) are considerably larger than the experimental appearance energies for the HCl elimination. The character of these transition states suggests that the HCl elimination may have a loose transition state (it is associated with an imaginary frequency of about $i100\text{ cm}^{-1}$). Location of the correct transition states turned out to be too complicated and because it was not in the focus of this study, it was not pursued further.

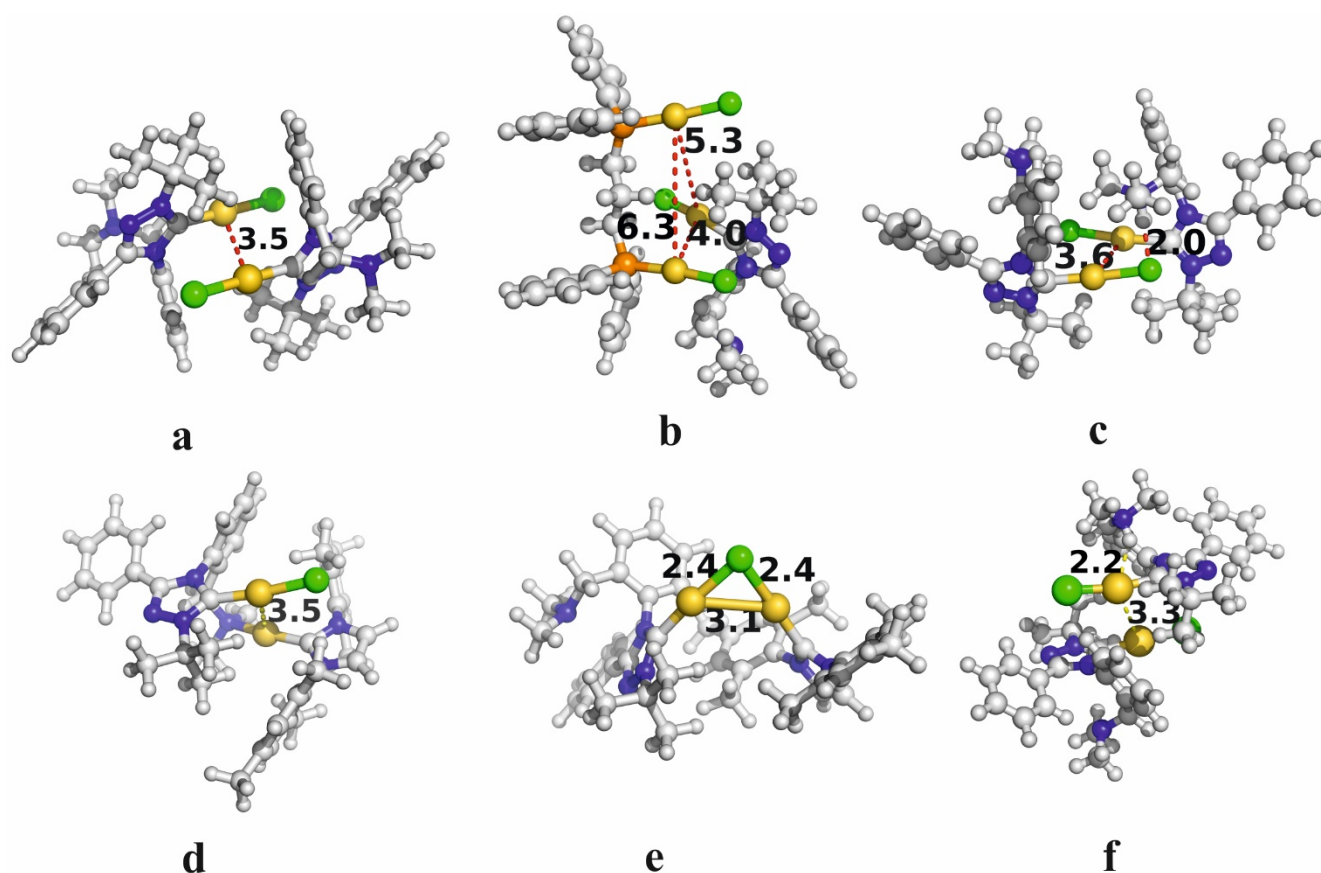


Figure 3. The equilibrium geometries of several representative structures studied in this work. The numbers given are internuclear distances in Ångströms. (a) the neutral $[(L^1)AuCl] \dots [(L^1)AuCl]$ species, the typical arrangement also observed in the crystal structures; (b) $[(L^1)AuCl] \dots [(L^7)AuCl]AuCl$; (c) $[(L^1H)AuCl]^+ \dots [(L^1)AuCl]$ charge-tagged (protonated) complex – internal rotation of the substituted phenyl ring leads to formation of a $Cl \dots H^+$ hydrogen bond; (d) $[(L^1H)AuCl]^+ \dots [(L^3)AuCl]$ – HCl dissociated; (e) $[(L^1H)AuCl]^+ \dots [(L^3)AuCl]$ with 1,2- μ -Cl arrangement, by $\sim 25\text{ kJ mol}^{-1}$ less stable than (e); (g) $[(L^1H)AuCl]^+ \dots [(L^1)AuCl]$ with the $Au(I) \dots H(+)$ interaction (c.f. Figure 1d). Full set of equilibrium geometries can be found in the Supporting Information.

5. Discussion

The agreement between computed and experimental values is crucial for further discussion. The calculated interaction enthalpies between the monomers in the $[(L^1H)AuCl]^+ \dots [(L^n)AuCl]$ clusters are on average $10 \text{ kJ}\cdot\text{mol}^{-1}$ (precisely $9.3 \text{ kJ}\cdot\text{mol}^{-1}$) smaller than their experimental counterparts (**Figure 4a**). As shown in **Table 2**, part of this systematic shift can be likely attributed to slight underestimation of the interaction energies at the SCS-MP2/CBS[D:T] level ($3\text{-}5 \text{ kJ}\cdot\text{mol}^{-1}$) or due to a small systematic shift in the experimental CID energies. Apart from the systematic shift of $10 \text{ kJ}\cdot\text{mol}^{-1}$, we consider the agreement between the computed and experimental data as excellent with maximum deviations within the experimental error bounds (**Figure 4, red line**). For neutral species, the SCS-MP2/CBS calculated values of interaction energies range between $71\text{-}105 \text{ kJ}\cdot\text{mol}^{-1}$ (ΔH_0). The reported ΔH_0 values can be viewed as experimentally and computationally calibrated interaction enthalpies (to within $10 \text{ kJ}\cdot\text{mol}^{-1}$) for the prototypical $\{Au \dots Au\}$ dimers and may represent benchmarks for experimental and computational studies dealing with aurophilic interactions.

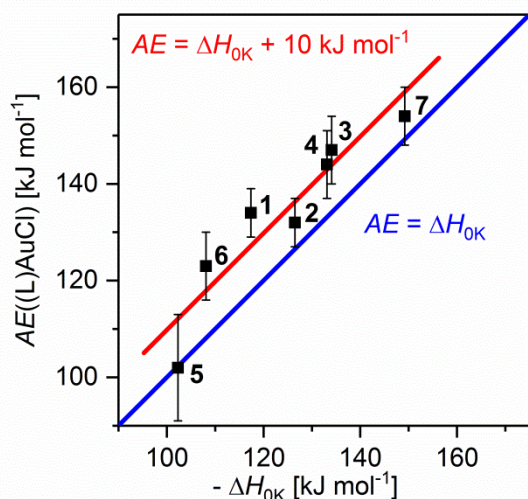


Figure 4. Correlation of the experimental appearance energies and SCS-MP2/CBS dissociation energies ($-\Delta H_{0K}$) of the $[(L^1H)AuCl]^+ \dots [(L^n)AuCl]$ dimers to monomers. The lines show the linear dependence with an offset of $10 \text{ kJ}\cdot\text{mol}^{-1}$ (red) or $0 \text{ kJ}\cdot\text{mol}^{-1}$ (blue). The data can be found in **Tables 1 and 3**.

En route to singling out “pure” metallophilic interactions from the overall interaction enthalpies, we compared the protonated systems with their neutral counterparts. An expected difference of $15\text{-}75 \text{ kJ}\cdot\text{mol}^{-1}$ was attributed to the charge-dipole term in the overall interaction energy. The interaction enthalpies for neutral systems can then be compared with the values calculated for model systems with

the corresponding NHC and PH₃ ligands (cf. **Figure 5**), at the geometries of the parent [(L¹)AuCl]...[(Lⁿ)AuCl] complexes, denoted as $\Delta E_{\text{int}}(\text{core})$ and listed in **Table 4**. The values obtained for the D_e values of [(L¹)AuCl]...[(Lⁿ)AuCl], $n = 1-6$, are 21-37 kJ mol⁻¹ more negative than those in the corresponding model complex. This additional interaction can originate either from the mutual interaction of the bulky ligands or from the electronic effects of the substituents on the ClAu(NHC)/(PH₃) core.

We further evaluated the inter-ligand interactions in the studied dimers by calculations, in which we removed the core (NHC)/(PH₃)AuCl units from the [(L¹)AuCl]...[(Lⁿ)AuCl] systems in the equilibrium geometry and capped the resulting valence vacancies by hydrogens (see **Figure 5**). The computed interaction energies are summarized in **Table 4**. The mutual interactions between the ligands are predicted to be attractive by 6-26 kJ mol⁻¹. Under the assumption of the additivity of these non-bonding ligand interactions with the interactions between the ClAu(NHC)/(PH₃) cores, the estimated interaction energies: $\Delta E_{\text{int}}(\text{L}...\text{L}') + \Delta E_{\text{int}}(\text{core})_{\text{est}}$ are compared with the values calculated for the full system. Intuitively, the difference between the two can be attributed to the ‘electronic’ effect of the bulky substituents on the strength of the interaction of the (NHC)/(PH₃)AuCl cores of the monomers. The electronic effects, estimated as $\Delta E_{\text{int}}(\text{el}) = \Delta E_{\text{int}} - (\Delta E_{\text{int}}(\text{L}...\text{L}') + \Delta E_{\text{int}}(\text{core}))$, are in all cases except one (L³) by 11-18 kJ mol⁻¹ stabilizing. For L³ ligand, these are close to neutral (3 kJ mol⁻¹ destabilizing). An in-depth analysis of the observed effect is beyond the scope of this work.

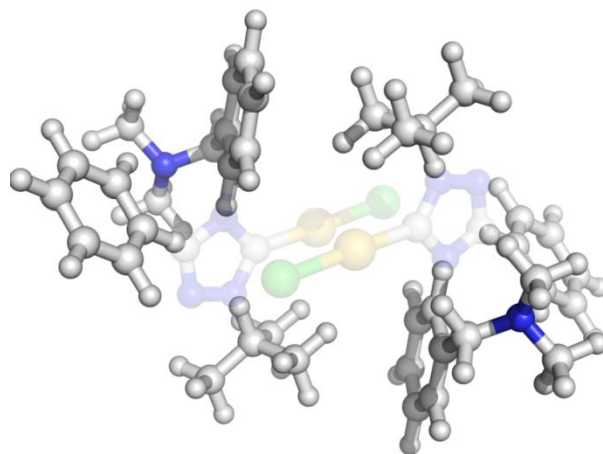


Figure 5: The geometry used to calculate the L...L’ inter-ligand interaction energy between the substituents on the respective (NHC)AuCl “cores” of the dimer. The substituents on the left side are considered as subsystem 1 whereas the substituents on the right side (originally on the second monomer) form subsystem 2.

Table 4. The calculated intra-ligand interaction energies ($D_e = \Delta E_{\text{int}}$; SCS-MP2/CBS, BSSE corrected) for the $[(L^1)\text{AuCl}] \dots [(L^n)\text{AuCl}]$ dimers ($n = 1-6$) studied.^a

	ΔE_{int}	$\Delta E_{\text{int}}(\text{core})$	$\Delta E_{\text{int}}(L^1 \dots L^n)$	$\Delta E_{\text{int}}(L^1 \dots L^n) + \Delta E_{\text{int}}(\text{core})$	$\Delta E_{\text{int}} - (\Delta E_{\text{int}}(L^1 \dots L^n) + \Delta E_{\text{int}}(\text{core}))$
L¹	-104.8	-74.2	-16.6	-90.8	-14.0
L²	-109.3	-74.2	-17.5	-91.7	-17.6
L³	-85.5	-62.9	-26.3	-89.2	3.7
L⁴	-91.7	-59.0	-22.0	-81.0	-10.7
L⁵	-86.7	-65.8	-6.3	-72.1	-14.6
L⁶	-90.5	-53.6	-18.8	-72.4	-18.1

^a All values are in kJ mol^{-1} (negative values indicate an attractive interaction)

Another simple computational experiment – inspired by the work of Straka and Pyykkö⁵⁶ - was the rotation of the monomers in the model systems by 90° around the Au-Au axis (L-Au...Au, Au...Au-L' bond angles and L-Au...Au-L' torsion angle were constrained to 90°). The perpendicular arrangement of the units cancels the leading dipole-dipole term. The investigated three model systems only ($[(\text{N}_2\text{C})\text{AuCl}]_2$, $[(\text{N}_2\text{C})\text{AuCl}] \dots [(\text{H}_3\text{P})\text{AuCl}]$, and $[(\text{H}_3\text{P})\text{AuCl}]_2$), because the bulky ligands in the $[(L^1)\text{Au-X}] \dots [(L^n)\text{AuX}]$ structures do not allow for the 90° rotation. The computed SCS-MP2/CBS[D:T, T:Q] interaction energies are -23 to -30 kJ mol^{-1} (Table 2). These values include the higher multipoles and dispersion interactions and in our opinion represent 'pure' metallophilic interactions. Therefore, it can be concluded that the metallophilic interactions are expected to be 20-30 kJ mol^{-1} and they account for ~30% of the overall interaction energy in the neutral $[(L^1)\text{AuX}] \dots [(L^n)\text{AuX}]$ dimers.

Finally, the interesting question is whether the metallophilic interactions are the primary determinants of the molecular structures of the gold(I) dimers, such as those studied in this work. In order to partially address this question, the studied systems were subjected to energy minimization using the Hartree-Fock method which presumably lacks the dispersion energy terms and the def2-SVP basis set. We found that all of the structures more or less remained in their antiparallel orientations (c.f. Supporting Information for all equilibrium geometries). Quite expectedly, the Au...Au distances increased (by 0.75-1 Å), whereas other structural features, such as the mutual orientation of the ligands,

were similar to the PBE-D3/def2-SVP equilibrium geometries (which were almost identical to available crystal structures).

6. Concluding remarks

We present the first experimental assessment of the magnitude of the aurophilic interactions. The binding energies between the monomers in the $[(L^1H)AuCl]^+ \dots [(L^n)AuCl]$ dimers were determined by collision induced dissociation experiments. The data were complemented by quantum chemical calculations calibrated against the CCSD(T) level with corrections for basis set incompleteness effects. The experimental binding energies show a systematic shift of approximately 10 kJ mol^{-1} with respect to the theoretical values. Allowing for this shift, partially attributed to the $\sim 3\text{-}5 \text{ kJ mol}^{-1}$ underestimated SCS-MP2/CBS[D:T] values, the agreement between the two enables us to quantify the metalophilicity and to discuss its role in the structure of gold(I) clusters. Our experimental and theoretical findings confirm the overall importance of the aurophilic interactions accounting for $\sim 25\text{-}30 \text{ kJ mol}^{-1}$ in the overall interaction energies of the real gold(I) dimers. This value is comparable or even greater than strong hydrogen bonds. However, structures of polynuclear gold(I) complexes may be determined also by other factors as shown by “switching off” the metalophilicity in the model calculations of the compounds studied. Borrowing a certain amount of *licentia poetica* for the gold(I) dimers studied we conclude that “*all that glitters is not gold*, but it matters once they hold.”

ASSOCIATED CONTENT

Supporting Information. Further experimental details (energy resolution –Figure S1; zero-pressure extrapolation – Figure S2; ion preparation – Figure S3; L-CID modelling of all data – Figures S4 – S10 and Tables S1, S2 Figures S1-S11), detailed description of the modification of the L-CID program (Figures S13 – S17, Tables S3 – S6), representative structures of the model compounds (Figure S12) and all equilibrium geometries of the compounds studied (separate SI text file) and all computed primary energetic data (TableSI_Energies).

Acknowledgment. We thank the referees for their suggestions that enabled us to substantially improve our work. The project was supported by the Grant Agency of the Czech Republic (17-24155S) and European Research Council (ERC CoG IsoMS No. 682275).

References

- (1) Sculfort, S.; Braunstein, P.: Intramolecular d^{10} - d^{10} interactions in heterometallic clusters of the transition metals. *Chem. Soc. Rev.* **2011**, *40*, 2741-2760.
- (2) Lin, J. C. Y.; Huang, R. T. W.; Lee, C. S.; Bhattacharyya, A.; Hwang, W. S.; Lin, I. J. B.: Coinage metal-N-heterocyclic carbene complexes. *Chem. Rev.* **2009**, *109*, 3561-3598.
- (3) Schmidbaur, H.; Graf, W.; Müller, G.: Weak Intramolecular Bonding Relationships - The Conformation-Determining Attractive Interaction Between Gold(I) Centers. *Angew. Chem., Int. Ed.* **1988**, *27*, 417-419.
- (4) Schmidbaur, H.; Scherbaum, F.; Huber, B.; Müller, G.: Polyauriomethane Compounds. *Angew. Chem., Int. Ed.* **1988**, *27*, 419-421.
- (5) Scherbaum, F.; Grohmann, A.; Huber, B.; Krueger, C.; Schmidbaur, H.: "Aurophilicity" as a Consequence of Relativistic Effects: The Hexakis(triphenylphosphaneaurio)methane Dication $[(Ph_3PAu)_6C]^{2+}$. *Angew. Chem. Int. Ed.* **1988**, *27*, 1544-1546.
- (6) Schmidbaur, H.; Schier, A.: A briefing on aurophilicity. *Chem. Soc. Rev.* **2008**, *37*, 1931-1951.
- (7) Schmidbaur, H.; Schier, A.: Aurophilic interactions as a subject of current research: an up-date. *Chem. Soc. Rev.* **2012**, *41*, 370-412.
- (8) Pyykkö, P.: Theoretical chemistry of gold. III *Chem. Soc. Rev.* **2008**, *37*, 1967-1997.
- (9) Xiong, X. G.; Xu, W. H.; Li, J.; Pyykkö, P.: Aspects of bonding in small gold clusters. *Int. J. Mass Spectrom.* **2013**, *354*, 15-18.
- (10) *see e.g.* Kishimura, A.; Yamashita, T.; Aida, T.: Phosphorescent Organogels via "Metallophilic" Interactions for Reversible RGB-Color Switching. *J. Am. Chem. Soc.* **2005**, *127*, 179-183.
- (11) Weaver, J.; Gaillard, S.; Toyé, C.; Macpherson, S.; Nolan, S. P.; Riches, A.: Cytotoxicity of Gold(I) N-Heterocyclic Carbene Complexes Assessed by Using Human Tumor Cell Lines. *Chem. Eur. J.* **2011**, *17*, 6620-6624.
- (12) Rubbiani, R.; Can, S.; Kitanovic, I.; Alborzina, H.; Stefanopoulou, M.; Kokoschka, M.; Mönchgesang, S.; Sheldrick, W. S.; Wölfl, S.; Ott, I.: Comparative in vitro evaluation of N-heterocyclic carbene gold(I) complexes of the benzimidazolylidene type. *J. Med. Chem.* **2011**, *54*, 8646-8657.
- (13) Oehninger, L.; Rubbiani, R.; Ott, I.: N-Heterocyclic carbene metal complexes in medicinal chemistry. *Dalton Trans.* **2013**, *42*, 3269-3284.
- (14) Turek, J.; Růžičková, Z.; Tloušťová, E.; Mertlíková-Kaiserová, H.; Günterová, J.; Rulíšek, L.; Růžička, A.: 1,2,4-Triazole-based N-heterocyclic carbene complexes of gold(I): synthesis, characterization and biological activity. *Appl. Organometal. Chem.* **2016**, *30*, 318-322.

- (15) Echavarren, A. M.; Hashmi, A. S. K.; Toste, F. D.: Gold Catalysis – Steadily Increasing in Importance. *Adv. Synth. Catal.* **2016**, 358, 1347-1347.
- (16) Marion, N.; Nolan, S. P.: N-heterocyclic carbenes in gold catalysis. *Chem. Soc. Rev.* **2008**, 37, 1776-1782.
- (17) Roithová, J.; Janková, Š.; Jašíková, L.; Váňa, J.; Hybelbauerová, S.: Gold-gold cooperation in the addition of methanol to alkynes. *Angew. Chem., Int. Ed.* **2012**, 51, 8378-8382.
- (18) Shu, X.-Z.; Nguyen, S. C.; He, Y.; Oba, F.; Zhang, Q.; Canlas, C.; Somorjai, G. A.; Alivisatos, A. P.; Toste, F. D.: Silica-Supported Cationic Gold(I) Complexes as Heterogeneous Catalysts for Regio- and Enantioselective Lactonization Reactions *J. Am. Chem. Soc.* **2015**, 137, 7083-7086.
- (19) Tkatchouk, E.; Mankad, N. P.; Benitez, D.; Goddard, W. A.; Toste, F. D.: Two Metals Are Better Than One in the Gold Catalyzed Oxidative Heteroarylation of Alkenes. *J. Am. Chem. Soc.* **2011**, 133, 14293-14300.
- (20) Larsen, M. H.; Houk, K. N.; Hashmi, A. S. K.: Dual Gold Catalysis: Step-Wise Catalyst Transfer via Dinuclear Clusters. *J. Am. Chem. Soc.* **2015**, 137, 10668-10676.
- (21) Zheng, Z.; Wang, Z.; Wang, Y.; Zhang, L.: Au-Catalysed oxidative cyclisation. *Chem. Soc. Rev.* **2016**, 45, 4448-4458.
- (22) Asiri, A. M.; Hashmi, A. S. K.: Gold-catalysed reactions of diynes. *Chem. Soc. Rev.* **2016**, 45, 4471-4503.
- (23) Harris, R. J.; Widenhoefer, R. A.: Gold carbenes, gold-stabilized carbocations, and cationic intermediates relevant to gold-catalysed enyne cycloaddition. *Chem. Soc. Rev.* **2016**, 45, 4533-4551.
- (24) Obradors, C.; Echavarren, A. M.: Intriguing mechanistic labyrinths in gold(I) catalysis. *Chem. Commun.* **2014**, 50, 16-28.
- (25) Pyykkö, P.; Runeberg, N.; Mendizabal, F.: Theory of the d^{10} - d^{10} Closed-Shell Attraction: 1. Dimers Near Equilibrium. *Chem. Eur. J.* **1997**, 3, 1451-1457.
- (26) Muñiz, J.; Wang, C.; Pyykkö, P.: Aurophilicity: The effect of the neutral ligand L on $[ClAuL]_2$ systems. *Chem. Eur. J.* **2011**, 17, 368-377.
- (27) Andrejić, M.; Mata, R. A.: Study of ligand effects in aurophilic interactions using local correlation methods. *Phys. Chem. Chem. Phys.* **2013**, 15, 18115-18122.
- (28) Pinter, B.; Broeckert, L.; Turek, J.; Růžička, A.; De Proft, F.: Dimers of N-Heterocyclic Carbene Copper, Silver, and Gold Halides: Probing Metallophilic Interactions through Electron Density Based Concepts. *Chem. Eur. J.* **2014**, 20, 734-744.
- (29) (a) Armentrout, P. B.; Ervin, K. M.; Rodgers, M. T.: Statistical Rate Theory and Kinetic Energy-Resolved Ion Chemistry: Theory and Applications. *J. Phys. Chem. A* **2008**, 112, 10071-10085. (b) Amicangelo, J. C.; Armentrout, P. B.: Relative and absolute bond dissociation energies of sodium cation-alcohol complexes determined using competitive collision-induced dissociation experiments. *Int. J. Mass Spectrom.* **2011**, 301, 45-54.

- (30) Narancic, S.; Bach, A.; Chen, P.: Simple Fitting of Energy-Resolved Reactive Cross Sections in Threshold Collision-Induced Dissociation (T-CID) Experiments. *J. Phys. Chem. A* **2007**, *111*, 7006-7013.
- (31) (a) Turek, J.; Panov, I.; Horáček, M.; Černošek, Z.; Padělková, Z.; Růžička, A.: Amino Group Functionalized N-Heterocyclic 1,2,4-Triazole-Derived Carbenes: Structural Diversity of Rhodium(I) Complexes. *Organometallics*, **2013**, *32*, 7234-7240. (b) Turek, J.; Panov, I.; Semler, M.; Štěpnička, P.; De Proft, F.; Padělková, Z.; Růžička, A.: Palladium(II) Complexes of 1,2,4-Triazole-Based N-Heterocyclic Carbenes: Synthesis, Structure, and Catalytic Activity. *Organometallics*, **2014**, *33*, 3108-3118.
- (32) Ducháčková, L.; Roithová, J.: The Interaction of Zinc(II) and Hydroxamic Acids and a Metal-Triggered Lossen Rearrangement. *Chem. Eur. J.* **2009**, *15*, 13399-13405.
- (33) Jašíková, L.; Roithová, J.: Interaction of the Gold(I) Cation $\text{Au}(\text{PMe}_3)^+$ with Unsaturated Hydrocarbons *Organometallics* **2012**, *31*, 1935-1942.
- (34) Note that Lorentzian shape of the kinetic energy distribution is a consequence of quadrupolar field that influences the ion transmission.
- (35) Jašík, J.; Žabka, J.; Roithová, J.; Gerlich, D.: Infrared spectroscopy of trapped molecular dications below 4 K. *Int. J. Mass Spectrom.* **2013**, *354–355*, 204–210.
- (36) Roithová, J.; Gray, A.; Andris, E.; Jašík, J.; Gerlich, D.: Helium Tagging Infrared Photodissociation Spectroscopy of Reactive Ions. *Acc. Chem. Res.* **2016**, *49*, 223–230.
- (37) TURBOMOLE V7.0 2015, a development of University of Karlsruhe and Forschungszentrum Karlsruhe GmbH, 1989-2007, TURBOMOLE GmbH, since 2007; available from <http://www.turbomole.com>.
- (38) Perdew, J. P.; Burke, K.; Ernzerhof, M.: Generalized Gradient Approximation Made Simple. *Phys. Rev. Lett.*, **1996**, *77*, 3865-3868.
- (39) (a) Grimme, S.; Antony, J.; Ehrlich, S.; Krieg, H.: A consistent and accurate ab initio parametrization of density functional dispersion correction (DFT-D) for the 94 elements H-Pu. *J. Chem. Phys.* **2010**, *132*, 154104. (b) Grimme, S.; Hansen, A.; Brandenburg, J. G.; Bannwarth, C.: Dispersion-Corrected Mean-Field Electronic Structure Methods. *Chem. Rev.*, **2016**, *116*, 5105–5154.
- (40) Weigend, F.; Ahlrichs, R.: Balanced basis sets of split valence, triple zeta valence and quadruple zeta valence quality for H to Rn: Design and assessment of accuracy. *Phys. Chem. Chem. Phys.* **2005**, *7*, 3297-3305.
- (41) Schäfer, A.; Huber, C.; Ahlrichs, R.: Fully optimized contracted Gaussian basis sets of triple zeta valence quality for atoms Li to Kr. *J. Chem. Phys.* **1994**, *100*, 5829-5835.
- (42) Tao, J. M.; Perdew, J. P.; Staroverov, V. N.; Scuseria, G. E.: Climbing the density functional ladder: nonempirical meta-generalized gradient approximation designed for molecules and solids. *Phys. Rev. Lett.* **2003**, *91*, 146401.
- (43) (a) Becke, A. D.: Density-functional exchange-energy approximation with correct asymptotic behavior. *Phys. Rev. A* **1988**, *38*, 3098-3100. (b) Lee, C.; Yang, W.; Parr, R. G.: Development of the Colle-Salvetti correlation-energy formula into a functional of the electron density. *Phys. Rev. B* **1988**, *37*, 785-789. (c) Becke, A. D.: Density-functional thermochemistry. III. The role

- of exact exchange. *J. Chem. Phys.* **1993**, *98*, 5648-5652. (d) Vosko, S. H.; Wilk, L.; Nusair, M.: Accurate spin-dependent electron liquid correlation energies for local spin density calculations: a critical analysis. *Can. J. Phys.* **1980**, *58*, 1200-1211.
- (44) Grimme, S.: Improved second-order Møller–Plesset perturbation theory by separate scaling of parallel- and antiparallel-spin pair correlation energies. *J. Chem. Phys.* **2003**, *118*, 9095-9102.
- (45) Woon, D. E.; Dunning, T. H.; Jr.: Gaussian basis sets for use in correlated molecular calculations. III. The atoms aluminum through argon. *J. Chem. Phys.* **1993**, *98*, 1358-1371.
- (46) Halkier, A.; Helgaker, T.; Jørgensen, P.; Klopper, W.; Koch, H.; Olsen, J.; Wilson, A. K.: Basis-set convergence in correlated calculations on Ne, N₂, and H₂O. *Chem. Phys. Lett.* **1998**, *286*, 243–252.
- (47) Kendall, R. A.; Dunning, T. H., Jr.; Harrison, R. J.: Electron Affinities of the First-Row Atoms Revisited. Systematic Basis Sets and Wave Functions. *J. Chem. Phys.* **1992**, *96*, 6796-6806.
- (48) Eichkorn, K.; Treutler, O.; Öhm, H.; Häser, M.; Ahlrichs, R.: Auxiliary basis sets to approximate Coulomb potentials. *Chem. Phys. Lett.* **1995**, *240*, 283-290.
- (49) Eichkorn, K.; Weigen, F.; Treutler, O.; Ahlrichs, R.: Auxiliary basis sets for main row atoms and transition metals and their use to approximate Coulomb potentials. *Theor. Chim. Acta* **1997**, *97*, 119-124.
- (50) Jensen, F. *Introduction to Computational Chemistry*; John Wiley & Sons: New York, 1999.
- (51) (a) J. Schulz, L. Jašíková, A. Škríba, J. Roithová, *J. Am. Chem. Soc.* **2014**, *136*, 11513 – 11523. (b) J. Schulz, J. Jašík, A. Gray, J. Roithová, *Chem. Eur. J.* **2016**, *22*, 9827 –9834.
- (52) (a) Moret, M. E.; Serra, D. Bach, A.; Chen, P.: Transmetalation Supported by a Pt-II-Cu-I Bond. *Angew. Chem. Int. Ed.* **2010**, *49*, 2873-2877. (b) Serra, D.; Moret, M. E.; Chen, P.: Transmetalation of Methyl Groups Supported by Pt-II-Au-I Bonds in the Gas Phase, in Silico, and in Solution. *J. Am. Chem. Soc.* **2011**, *133*, 8914-8926. (c) Oeschger, R. J.; Ringger, D. H.; Chen, P.: Gas-Phase Investigations on the Transmetalation Step in Sonogashira Reactions. *Organometallics*, **2015**, *34*, 3888-3892. (d) Oeschger, R. J.; Chen, P. *J. Am. Chem. Soc.* **2017**, *139*, 1069–1072.
- (53) Pollice, R.; Bot, M.; Kobylanskii, I. J.; Shenderovich, I.; Chen, P. Attenuation of London Dispersion in Dichloromethane Solutions. *J. Am. Chem. Soc.* **2017**, *139*, 13126–13140.
- (54) Ray, L.; Shaikh, M. M.; Ghosh. P.: Shorter argentophilic interaction than aurophilic interaction in a pair of dimeric {(NHC)MCl}₂ (M= Ag, Au) complexes supported over a N/O-Functionalized N-Heterocyclic Carbene (NHC) ligand. *Inorg. Chem.* **2008**, *47*, 230–240.
- (55) Turek, J.; Panov, I.; Švec, P.; Růžičková, Z.; Růžička, A.: Non-covalent interactions in coinage metal complexes of 1,2,4-triazole-based N-heterocyclic carbenes. *Dalton Trans.* **2014**, *43*, 15465-15474.
- (56) Pyykkö, P.; Straka, M.: Ab initio studies of the dimers (HgH₂)₂ and (HgMe₂)₂. Metallophilic attraction and the van der Waals radii of mercury. *Phys. Chem. Chem. Phys.* **2000**, *2*, 2489-2493.
- (57) Riplinger, C.; Neese, F. An efficient and near linear scaling pair natural orbital based local coupled cluster method. *J. Chem. Phys.* **2013**, *138*, 034106.

- (58) Řezáč, J.: Cuby: An integrative framework for computational chemistry. *J. Comput. Chem.* **2016**, 37, 1230–1237.

For Table of Contents Only

